Journal of Colloid and Interface Science **235,** 80–88 (2001)
doi:10.1006/jcis.2000.7249, available online at http://www.idealibrary.com on IDEAL®

X-ray Absorption Spectroscopic Investigation of Arsenite and Arsenate Adsorption at the Aluminum Oxide–Water Interface

Yuji Arai,[1] Evert J. Elzinga, and Donald L. Sparks

Department of Plant and Soil Sciences, University of Delaware, Newark Delaware 19717-1303

Received April 13, 2000; accepted September 28, 2000

We investigated the As(III) and As(V) adsorption complexes forming at the γ-Al_2O_3/water interface as a function of pH and ionic strength (*I*), using a combination of adsorption envelopes, electrophoretic mobility (EM) measurements, and X-ray absorption spectroscopy (XAS). The As adsorption envelopes show that (1) As(III) adsorption increases with increasing pH and is insensitive to *I* changes (0.01 and 0.8 M $NaNO_3$) at pH 3–4.5, while adsorption decreases with increasing *I* between pH 4.5 and 9.0, and (2) As(V) adsorption decreases with increasing pH and is insensitive to *I* changes at pH 3.5–10. The EM measurements show that As(III) adsorption does not significantly change the EM values of γ-Al_2O_3 suspension in 0.1 M $NaNO_3$ at pH 4–8, whereas As(V) adsorption lowered the EM values at pH 4–10. The EXAFS data indicate that both As(III) and As(V) form inner-sphere complexes with a bidentate binuclear configuration, as evidenced by a As(III)–Al bond distance of ≅3.22 Å and a As(V)–Al bond distance of ≅3.11 Å. The As(III) XANES spectra, however, show that outer-sphere complexes are formed in addition to inner-sphere complexes and that the importance of outer-sphere As(III) complexes increases with increasing pH (5.5 to 8) and with decreasing *I*. In short, the data indicate for As(III) that inner- and outer-sphere adsorption coexist whereas for As(V) inner-sphere complexes are predominant under our experimental conditions.

Key Words: **arsenic; γ-Al_2O_3; adsorption mechanisms; XAS; electrophoretic mobility; oxide–water interface.**

INTRODUCTION

Arsenic (As) is a ubiquitous toxic metalloid in the soil/water environment due to natural geologic processes (volcanic eruption and weathering) and anthropogenic sources (mining, industrial processes, and agricultural practices). The average total As content in uncontaminated soils is approximately 5 ppm (1–3); however, the total As levels in fields that received As-containing pesticides and defoliants range from 5 to 2553 ppm (4) In aquatic environments, typical concentrations of total As range from 1 ppb to 3 ppm (5–8).

The United States Environmental Protection Agency recently proposed lowering the maximum concentration level (MCL) for total As in drinking water from 50 to 5 ppb. This new MCL raises serious concerns about human and ecological health in many parts of the United States where the As levels currently are above 5 ppb. Inorganic As has four oxidation states: +5, +3, 0, and −3. In the soil/water environment, it is mainly present in the +3 and +5 oxidation states. In reduced environments, arsenious acid is a common As(III) aqueous species, whereas oxidized environments contain more As(V) aqueous species. These two aqueous species may adsorb onto inorganic and organic soil components and or precipitate in a variety of forms. The pK_a values of As(III) and As(V) (As(III): $pK_1 = 9.22$ and $pK_2 = 12.13$; As(V): $pK_1 = 2.20$, $pK_2 = 6.97$, and $pK_3 = 13.4$ (9)) predict that the predominant solution species at typical environmental pH values (4–8) would be $As(OH)_3^0(aq)$ for As(III) and $H_2AsO_4^-$ and $HAsO_4^{2-}$ for As(V).

The environmental fate of As in subsurface environments is highly dependent on the As speciation, pH, ionic strength, and the presence of adsorbents such as metal oxides and phyllosilicates. In acid to alkaline environments, arsenic can be adsorbed onto variable-charge mineral surfaces by inner-sphere and/or outer-sphere complexation. Inner-sphere complexes form via a ligand exchange reaction with a surface functional group, and as a result, no water molecules are present between surface functional groups and the adsorbate ions. Outer-sphere complexes from mainly by electrostatic interactions and contain more than one water molecule between the adsorbate and the adsorbent functional groups (10).

Several researchers have investigated As adsorption on soil minerals using macroscopic techniques and surface complexation models. As(V) adsorption studies on metal oxides have shown that As(V) is strongly adsorbed on amorphous $Al(OH)_3$, α-Al_2O_3, ferrihydrite, and hematite at acidic pH (pH 3–5) and that adsorption gradually decreases with increasing pH between pH 6–10 (1–3). Conversely, As(III) adsorption on ferrihydrite, goethite, kaolinite, illite, montmorillonite, and amorphous aluminum oxide has been shown to increase gradually with increasing pH from 3.5 up to 8–9 (2, 11, 12). An application of the triple-layer model to As(V) adsorption on amorphous iron oxide at pH 4–10 suggested the formation of inner-sphere monodentate mononuclear species (13). The constant capacitance model has been used to describe As(III) adsorption behavior on goethite, assuming the predominant formation of bidentate binuclear surface complexes (11).

[1] To whom correspondence should be addressed. E-mail: ugarai@udel.edu.

0021-9797/01 $35.00

X-ray absorption fine structure spectroscopic (XAFS) studies have shown the formation of both inner-sphere bidentate binuclear and monodentate As(V) complexes on ferrihydrite and goethite at pH 6–8 (14, 15). Attenuated total reflectance Fourier transform infrared spectroscopic (ATR-FTIR) studies, electrophoretic mobility (EM) measurements, and titration studies also suggested inner-sphere adsorption mechanisms of As(V) and As(III) on ferrihydrite (16). *Ex situ* ATR-FTIR studies indicated that both As(III) and As(V) adsorbed to the goethite surface as inner-sphere bridging bidentate complexes at pH 3–8.5 (17). An *in situ* EXAFS investigation of As(III) adsorption at the goethite/water interface reported a bidentate binuclear bridging configuration with an average As–Fe distance of 3.378 ± 0.014 Å (11).

Unfortunately, there are no *in situ* spectroscopic studies of arsenic adsorption at the aluminum oxide/water interface. Aluminum oxides such as gibbsite may play an important role in As retention in soil/water environments because their aluminol functional groups serve as dynamic sinks for various oxyanions (18). A strong correlation between As(V) retention with ammonium oxalate extractable Al indicated the importance of As(V) fixation by amorphous aluminum oxides in soils (19, 20).

In this study, we investigated the complexation of As(III) and As(V) at the aluminum oxide/water interface as a function of pH and ionic strength using a combination of adsorption envelopes, electrophoretic mobility measurements, and X-ray absorption spectroscopy (XAS). We chose γ-Al_2O_3 (Degussa Corp., Akron, OH) as the adsorbate in this study because the surface of well-hydrated γ-Al_2O_3 (Degussa) is structurally similar to that of aluminum oxides (e.g., bayrite) in soils. ATR-FTIR and diffuse reflectance (DR) Fourier-transformed infrared (FTIR) spectroscopic investigations showed that the surface of γ-Al_2O_3 transformed into the bayerite polymorph upon aging (21, 22).

MATERIALS AND REAGENTS

Total ignition and transmission electron microscopic analysis (TEM) of the γ-Al_2O_3 showed greater than 99.6% purity and an average particle radius of 13 nm (Degussa). The five-point Brunauer–Emmett–Teller (BET) surface area of the γ-Al_2O_3 was $\cong$90.1 $m^2\,g^{-1}$. The isoelectric point was $\cong$9.3, as determined by electrophoretic mobility measurements. ACS-grade sodium arsenate, $Na_2HAsO_4 \cdot 7H_2O$ (Baker), and sodium *m*-arsenite, $NaAsO_2$(Sigma), were used as sources of arsenic reagents. All reagents and samples were prepared with boiled DDI water in a N_2-filled glove box to minimize the competitive adsorption between As and carbonate species as well as potential As(III) oxidation by dissolved oxygen. The As(III) reagent was prepared in an acidic medium (pH $\cong$ 3 HNO_3 solution) to avoid auto-oxidation at alkaline pH.

METHODS

Adsorption Envelopes

Arsenic adsorption was studied as a function of *I* (0.01 and 0.8 M $NaNO_3$) and pH (3–10). The concentrations of γ-Al_2O_3 and arsenic were 5 g L^{-1} and 0.7 mM, respectively. Hydration of γ-Al_2O_3 adsorbent was effected in two steps. In the first step, 100 ml γ-Al_2O_3 suspensions were hydrated in 0.01 or 0.8 M $NaNO_3$ solutions for 7 days. The γ-Al_2O_3 material transformed into a bayerite polymorph during this hydration period, as was verified via ATR-FTIR analysis. Next, the pH of the suspensions was adjusted to values ranging between 3.75 and 9, using either 0.1 M HNO_3 or 0.1 M NaOH, and equilibrated for an additional 24 h. An appropriate amount of 5 mM As(III or V) stock solution was then added to achieve an initial As concentration of 0.7 mM. The samples were reacted for 20 h on an orbital shaker operating at 300 rpm. The final pH was measured in the N_2-filled glove box, and 30 mL of the suspension was removed and then centrifuged at 11,950 g for 5 min. The supernatant was filtered through 0.2-μm filter paper. The filtrates of the arsenite-reacted samples were treated with KIO_3 to induce the oxidation of As(III) to As(V). The total As(V) concentrations of the filtrates were measured by the ammonium molybdenum method described in Cummings *et al.* (23).

Electrophoretic Mobility Measurements

The EM measurements were performed on a Zeta-Meter system 3.0 (Zeta Meter, Inc., NY). To assure the accuracy in EM measurements, the instrument was calibrated by measuring a constant ζ potential (-29 ± 1 mV) of standard colloidal silica (Min-U-Sil) in distilled water. The suspension density of γ-Al_2O_3 was 0.25 g L^{-1}, and the background electrolyte was 0.1 M $NaNO_3$. Hydration of the γ-Al_2O_3 material was as described above. The EM measurements of the mineral suspensions were conducted at pH 4–10 for As(V) and at pH 4–8 for As(III). Measurements at each pH value were done in both the presence and the absence of 0.1 mM As(III) or 0.1 mM As(V). The narrower pH range for the As(III) system was chosen due to potential As(III) oxidation at a pH of >9.2 (12). The tracking times (s) of a total of ten particles were averaged, and the average values were used to estimate EM using the Helmholtz–Smoluchowski equation (24). The average particle radius of 13 nm and $I = 0.1$ M are within the Hückel and Helmholtz–Smoluchowski limits for estimating the EM values using the Helmholtz–Smoluchowski equation (24).

Synchrotron XAS Analysis

All XAS samples were prepared at 25($\pm$2)°C in a N_2-filled glove box using the same experimental methods as described above for preparation of the As adsorption envelopes. The arsenite samples were prepared at $I = 0.8$ and 0.01 M $NaNO_3$ and pH 5.5 and 8. The arsenate samples were prepared at pH 4, 8, and 10 at the same two *I* values used in the As(III) experiments.

The total sample volumes were 30 ml. The γ-Al_2O_3 suspensions were centrifuged at 11,950 g for 5 min and the wet paste was recovered for XAS analysis. The mass of residual As in the entrained solution represented at most 3.5% of the total adsorbed As, and therefore the contribution of entrained (nonadsorbed) As to the XAS spectra was negligible in all samples.

In addition to the As sorption samples, XAS spectra of As solutions (10 mM of sodium arsenite at pH 3.5 and sodium arsenate at pH 4.2) were collected as references for As(III) and As(V) outer-sphere complexes. According to the MINEQL+ chemical modeling speciation program (25), *the speciation of As in these solutions was near 100% As(OH)$_3$(aq) and 100%; $H_2AsO_4^-$(aq) at these pHs.* The spectra of aqueous As(V) collected at pH 4, 8, and 10 were all the same; therefore, the XANES and the EXAFS results were not sensitive to As(V) protonation. The solution and paste samples were loaded in Teflon sample holders inside the glove box, which were then sealed with Kapton tape (CHR Industries) and stored in double ziplock bags containing a N_2 atmosphere. The samples were kept at $\cong$3–5°C without exposure to atmospheric air prior to XAS data collection.

Arsenic K-edge (11,867 eV) XAS spectra were collected on beamline X-11A at the National Synchrotron Light Source (NSLS), Brookhaven National Laboratory, Upton, NY. The electron storage ring was operated at 2.528 GeV with a current range of 130 to 300 mA. The XAS spectra were collected in fluorescence mode with a Lytle detector filled with Krypton gas. The ionization chamber (I_0) was filled with 90% N_2 and 10% Ar. As an internal standard, the arsenic K-edge of sodium arsenate salt was run simultaneously with adsorption samples to check for potential energy shifts during the run as well as possible As(III) oxidation during data collection. No oxidation of As(III) adsorbed at the γ-Al_2O_3 surface was observed. A Ge filter was used to remove elastically scattered radiation from the fluorescence emissions. The monochromator consisted of two parallel Si(111) crystals with a vertical entrance slit of 0.5 mm. The Teflon sample holder was oriented at 45° to the unfocused incident beam and was attached to a cold finger cooled by liquid nitrogen ($T = 77$ K). We performed data collection of the sorption samples at 77 K to minimize thermal disorder and possible oxidation of As(III) samples. For some samples, data collection was done at 298 K. Except for the signal-to-noise ratio, no differences were observed with the data collected at 77 K. The solution reference samples were scanned at 298 K. A total of three spectra were collected for the sorption samples, and one spectrum was collected for the solution samples.

XAS data reduction and analysis were performed with WinXas 1.1 (26) using the following procedures. First, three spectra (except for the solution samples) per sample were averaged. The averaged spectra were normalized with respect to E_0 determined from the second derivative of the raw spectra, and then the total atomic cross-sectional absorption was set to unity. A low-order polynomial function was fit to the pre-edge region and the post-edge region. Next, the data were converted from E space to k space and weighted by k^3 to compensate for dampening of the XAFS amplitude with increasing k space. Fourier transformation was then performed over the k-space range of 1.3 to 11.6 Å^{-1} to obtain the radial structural functions (RSF). Final fitting of the spectra was done on Fourier-transformed k^3 weighted spectra in R space. The FEFF7 code reference (27) was utilized to calculate single scattering theoretical spectra and phase shifts for As–O and As–Al backscatters using an input file based on the structural refinement of scorodite ($FeAsO_4 \cdot H_2O$)(28) with one Fe atom at 3.3376 Å replaced by Al. The amplitude reduction factor was 0.91. During fitting, the values of N and R of the As–O and As–Al shells as well as a single E_0 for all sets of backscattering atoms were allowed to vary. The Debye–Waller factors of the As–O shells were also allowed to vary, but those of the As–Al shells were fixed at 0.01 Å^2 for As(III) and 0.006 Å^2 for As(V). When allowed to vary, the Debeye–Waller factors of the As–Al shells showed no trends for different samples (e.g., as a function of pH or I), and we therefore used the average values (0.006 Å^2 for As(V) and 0.01 Å^2 for As(III)) in the final fitting procedure to reduce the number of free parameters. Error estimates for the As–O shells are $\pm$0.02 Å and $\pm$20% for the R and N values, respectively, based on fits to the aqueous standards and the scorodite reference compound. The N and R values for the more distant Al shells will be less accurate than those for the As–O shells, but we lacked an As–Al reference compound to make an accurate estimate of the errors. Based on the As–Fe shell fitting results of the scorodite reference compound, we estimate the errors to be at least $\pm$0.03 Å and $\pm$30% for $R_{\text{As–Al}}$ and $N_{\text{As–Al}}$, respectively.

The XANES spectra of the adsorption and solution samples were normalized with respect to the step height at the edge energies and compared to gain additional information regarding the local atomic structure of adsorbed As(III) and As(V) on the γ-Al_2O_3 surface.

RESULTS AND DISCUSSION

Adsorption Envelopes

Figure 1 shows the effects of ionic strength (I) on As(III) and As(V) adsorption envelopes. Arsenate adsorption appears to be insensitive to changes in I between pH 3 and 9.2. Approximately 90% of As(V) was removed at a pH of $\cong$5 at both I, and the net adsorption decreased to 25% with pH increases up to 10 (Fig. 1). Adsorption of As(III), however, was dependent on both I and pH: adsorption increased from 30 to 55% with increasing pH from 3.2 to 8.2 and decreased with increasing I within the same pH range (Fig. 1).

Hayes and co-workers proposed an indirect macroscopic method for distinguishing inner-sphere from outer-sphere complexes by examining I effects on adsorption envelopes coupled with the generalized triple-layer model (29). According to this method, the formation of inner-sphere complexes is not greatly affected by I, whereas the presence of outer-sphere complexes is indicated by changes in sorption with changing I due to

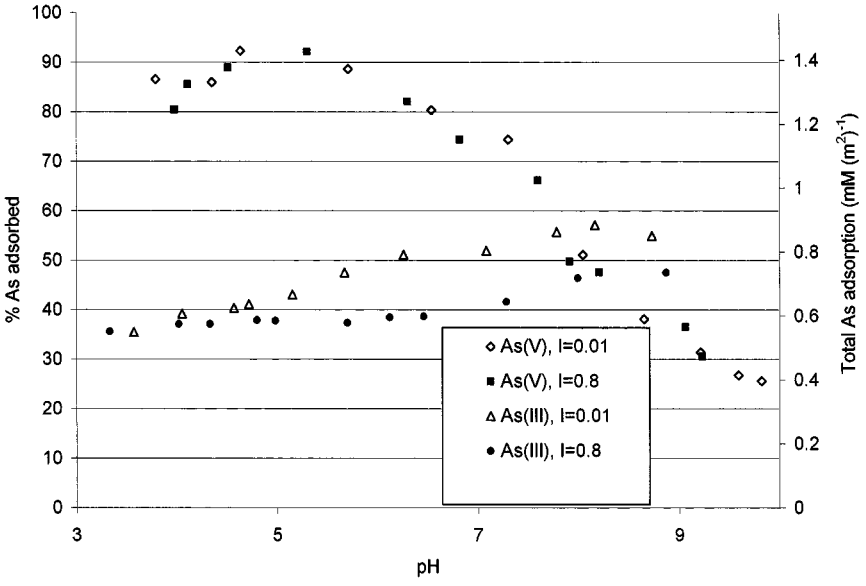

FIG. 1. Ionic strength effects on As(III and V)/γ-Al_2O_3 adsorption envelopes.

competitive adsorption with counteranions. Based on this theory, our data suggest that As(III) predominantly forms inner-sphere complexes at pH 3–4 and outer-sphere complexes form in the pH range 4.5–10, whereas As(V) predominantly forms inner-sphere complexes regardless of pH and *I*.

It is interesting to compare this data interpretation with the adsorption mechanisms that may be expected based on the pH-dependent As solution speciation and charge properties of aluminum oxide surfaces. The dissociation constants of As(III) and As(V) indicate that the predominant solution species are negatively charged As(V) species ($H_2AsO_4^-$ and or $HAsO_4^{2-}$) and uncharged As(III) species ($As(OH)_3$) at pH 3–9. The surface of the aluminum oxide in this pH range has a net positive charge due to its relatively high IEP ($\cong$9.3) (Fig. 2). Therefore, As(V) might adsorb on the γ-Al_2O_3 surface at a pH of <9.3 via electrostatic interactions (outer-sphere complexes), but at a pH of >9.3 predominantly inner-sphere complexation would be expected to occur. Similarly, electrostatic interactions and or ligand exchange reactions between As(III) and the γ-Al_2O_3 surface may occur at pH 3–9, whereas predominant inner-sphere adsorption is expected at a pH of >9.2 due to the development of negatively charged As(III) species ($pK_1 = 9.22$; $As(OH)_3 + H_2O = As(OH)_4^- + H^+$).

Based on the results of the *I*-dependent adsorption envelopes and the surface complexes predicted by pH-dependent characteristics of the adsorbents and the adsorbate, no conclusive statements on the As(III) and As(V) surface speciation can be made. Recent spectroscopic studies have shown that some metals and an oxyanion may form mixtures of inner- and outer-sphere complexes at metal oxide and clay mineral surfaces (30–32). We therefore performed EM measurements and XAS studies for further characterization of As complexation at the γ-aluminum oxide/water interface.

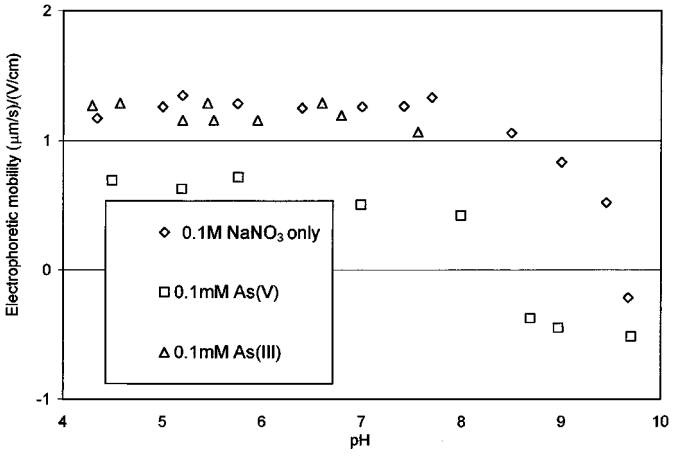

FIG. 2. Electrophoretic mobility measurements on γ-Al_2O_3 with and without 0.1 mM As(III or V). All systems contained 0.1 M $NaNO_3$.

Electrophoretic Mobility Measurements

According to Hunter electrophoretic mobility (EM) measurements are useful not only to obtain IEPs for colloidal materials but also to indirectly distinguish inner-sphere complexes from outer-sphere complexes (33). Nonspecific ion adsorption of indifferent electrolytes outside the shear plane (i.e., formation of outer-sphere complexes via van der Waals forces) generally does not affect the IEP but it could cause shifts in the value of EM if present at high concentrations of indifferent electrolyte (33). The shear plane is at the outer edge of the inner part of the double layer and near the outer Helmholtz plane or the Stern layer, depending on the models to describe the interface (33). Inner-sphere complexes generally cause shifts in both IEP and EM due to specific ion adsorption inside the shear plane (33). In some

cases, however, inner-sphere adsorption does not significantly affect the EM and IEP of the pure solid suspension (16, 33).

The electrophoretic mobility measurements indicated that sorption of As(V) (in a 0.1 M $NaNO_3$ background) lowered the EM between pH 4–10 and shifted the isoelectric point of the solid from ≅9.4 to ≅8.4 (Fig. 2). Adsorption of As(III), however, resulted in no significant change in EM between pH 4 and 8 (Fig. 2). These results agree with the EM measurements on amorphous $Al(OH)_3$ reacted with As(III and V) reported by Suarez *et al.* (16). A large shift in the point-of-zero charge (PZC) from pH 9.2 to 5.4 was observed in the presence of 1 mM As(V), whereas the same measurement with As(III) showed only a slight shift in PZC (16).

Based on the information above, our EM measurements suggest the formation of inner-sphere complexes for As(V) at pH 4–10. It is true that EM can be shifted by a physically adsorbed anion such as nitrate, but the nitrate concentration is constant in all EM measurements. If physical adsorption of nitrate is outcompeting the formation of outer-sphere As(V) complexes, we should observe the same EM values for the systems containing 0.1 M $NaNO_3$ in the presence and absence of 0.1 mM As(V), which is not the case (Fig. 2). Therefore, our experimental evidence (shifts in IEP and EM with 0.1 mM As(V) and 0.1 $NaNO_3$) suggests that As(V) is specifically adsorbed (i.e., forms inner-sphere complexes) at the γ-aluminum oxide/water interface.

Another explanation for the observed EM shift of the As(V)–γ-Al_2O_3 samples is the formation of aluminum–arsenate (surface) precipitates, which might mask the charge properties of the γ-Al_2O_3. However, speciation calculations in MINEQL+ predict that all samples were undersaturated with respect to $AlAsO_4 \cdot 2H_2O$(s). Calculations were based on the initial [As] = 0.7 mM and total dissolved Al concentrations ≅99 μM, which was the highest Al concentration measured in the supernatants of the samples before As was added. Additionally, our EXAFS data show no indication of the formation of such precipitates, as will be shown in a later section.

The fact that we do not observe a change in the EM value of γ-Al_2O_3 upon As(III) adsorption can be explained by either the formation of outer-sphere complexes and/or the formation of neutral inner-sphere complexes.

Arsenic XANES Analysis

The normalized XANES spectra of the As(III and V) adsorption samples and the reference arsenic solution samples are presented in Figs. 3 and 4. For the As(III)/γ-Al_2O_3 samples reacted at pH 8, there is a significant effect of ionic strength on the XANES spectra, whereas only a minor effect is observed at pH 5.5 (Fig. 3).

Comparison of the XANES spectra of the high and low *I* As(III) adsorption samples reacted at pH 8 to the spectrum of aqueous As(III)(Fig. 3) shows that the low *I* (0.01 M) adsorption sample has a similar overall oscillation pattern to the aqueous As(III) standard between 0 and 100 eV. The highest point in both spectra (at ≅+3 eV) is followed by a downward oscillation

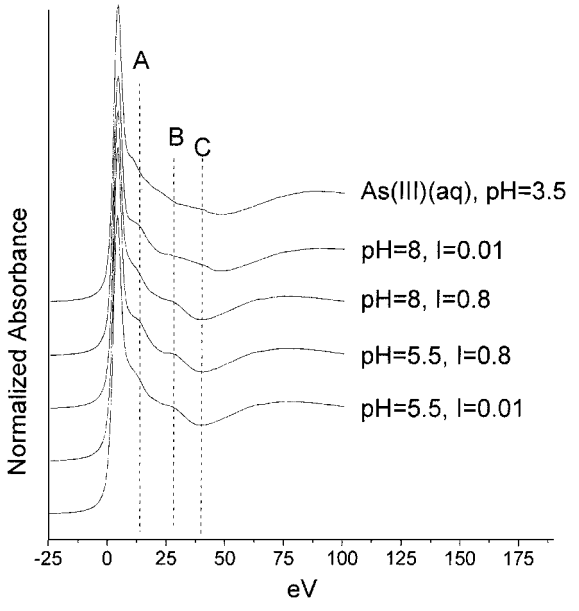

FIG. 3. XANES spectra of the As(III)–γ-Al_2O_3 and sodium As(III) solution samples.

between 3 and 50 eV. For the other three As(III) adsorption samples, the first downward oscillation is between 3 and ≅40 eV (indicated by a dashed line C in Fig. 3) and contains a well-resolved beat (indicated by a dashed line B in Fig. 3) at ≅27 eV. This beat is absent in the As(III)(aq) sample and not well resolved in the As(III)/γ-Al_2O_3 sample reacted at pH 8 and $I = 0.01$. A shoulder also occurs at ≅10 eV (indicated by dashed line A in Fig. 3) and is present in all spectra, but it is broader in the As(III) adsorption samples than in the aqueous As(III) spectrum.

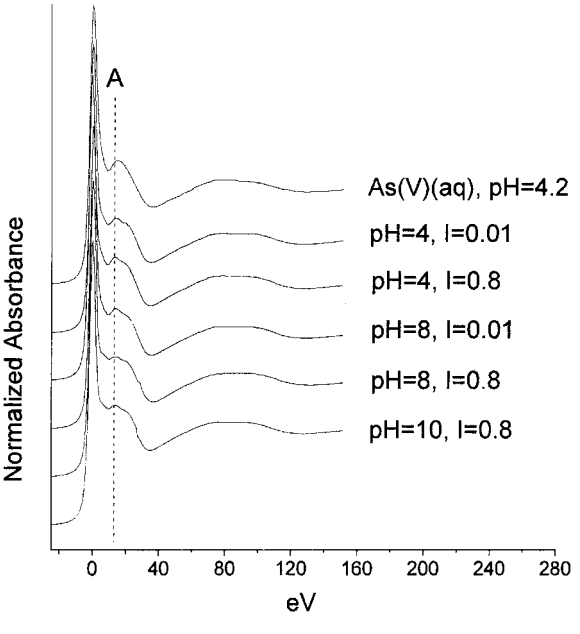

FIG. 4. XANES spectra of the As(V)–γ-Al_2O_3 and sodium As(V) solution samples.

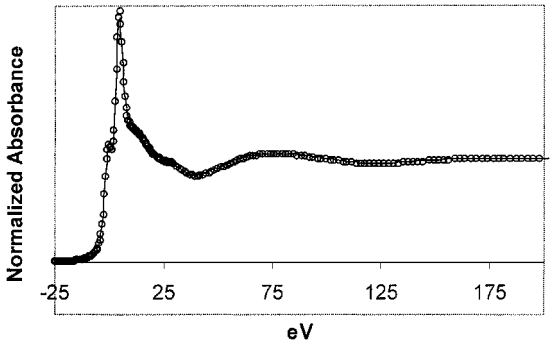

FIG. 5. Results of linear combinations (LC) of a XANES profile fit for As(III)/γ-Al_2O_3 adsorption sample (pH 8, $I = 0.01$). The solid line is the experimental data and the open circles represent the LC fit.

Overall, the spectrum of the sample reacted at pH 8 and $I = 0.01$ M appears to be intermediate between the aqueous As(III) spectrum and the spectra of the other As(III) adsorption samples; i.e., it contains features from both spectra. This indicates that this sample contains a mixture of inner-sphere and outer-sphere As(III) complexes, whereas the other samples contain mainly As(III) sorbed in an inner-sphere fashion. To substantiate the notion that the As(III)/γ-Al_2O_3 samples reacted at pH 8 and $I = 0.01$ M contains a mixture of outer-sphere and inner-sphere As(III) sorption complexes, the XANES spectrum of this sample was fit with a linear combination (LC) of spectra representative of inner- and outer-sphere complexes As(III) complexes (26). For the outer-sphere reference, we used the spectrum of a sodium arsenite solution (10 mM and pH 3.5). For the inner-sphere reference, we used the spectrum of the As(III)/γ-Al_2O_3 sample reacted at pH 5.5 and $I = 0.8$ M since it shows pronounced features of inner-sphere complexation (Fig. 2). As shown in Fig. 5, an excellent fit was obtained with relative contributions of inner-sphere and outer-sphere complexes of approximately 66 and 34%, respectively. Fits on the k^3-weighted χ spectrum of these samples gave similar results (not shown). These results support the notion that the sample reacted at pH 8 and $I = 0.01$ M contains a mixture of inner- and outer-sphere As(III) sorption complexes.

Our As(III) XANES results, which suggest the formation of both inner- and outer-sphere complexes at pH 8 and $I = 0.01$ M but only the formation of inner-sphere complexes at pH 5.5, are consistent with the results of the *I* effect on the As(III) adsorption envelopes (Fig. 1). At a pH of >5.5, lowering *I* resulted in increased As(III) adsorption, which indirectly suggested that outer-sphere As(III) complexation also occurs in this pH range, whereas the insensitivity of As(III) adsorption to *I* changes at a pH of <5 suggests the predominant formation of inner-sphere As(III) complexation (Fig. 1).

The EM measurements of As(III)-reacted γ-Al_2O_3 showed no significant change in the EM values of γ-Al_2O_3 between pH 4 and 8 compared to nonreacted γ-Al_2O_3 (Fig. 2). Combined with the As(III) XANES data, our EM data suggest that the As(III) inner-sphere complexes forming at the γ-Al_2O_3 are neutral, both at pH of <5.5, where they predominate, as well as at pH of >5.5, where they co-exist with outer-sphere As(III) surface complexes.

Unlike the As(III) samples, there were no significant differences in the XANES features in the As(V) adsorption samples reacted under different reaction conditions (Fig. 4). Moreover, the spectra of the sorption samples show distinct features different from the As(V)(aq) spectrum (Fig. 4). A peak at $\cong$18 eV (indicated by dashed line A) is sharp in an aqueous arsenate sample but the feature becomes broader in all adsorption samples. Our As(V) XANES data suggest As(V) inner-sphere complexation in all adsorption samples, regardless of pH and *I*. This result is consistent with the result of the adsorption envelope as a function of *I* and the EM measurements, which suggested the formation of As(V) inner-sphere complexes at the alumina surface (Figs. 1 and 2).

Arsenic K-edge EXAFS Analysis

Figures 6a and 7a show the background subtracted k^3-weighted χ functions of the As(III and V)/γ-Al_2O_3 samples

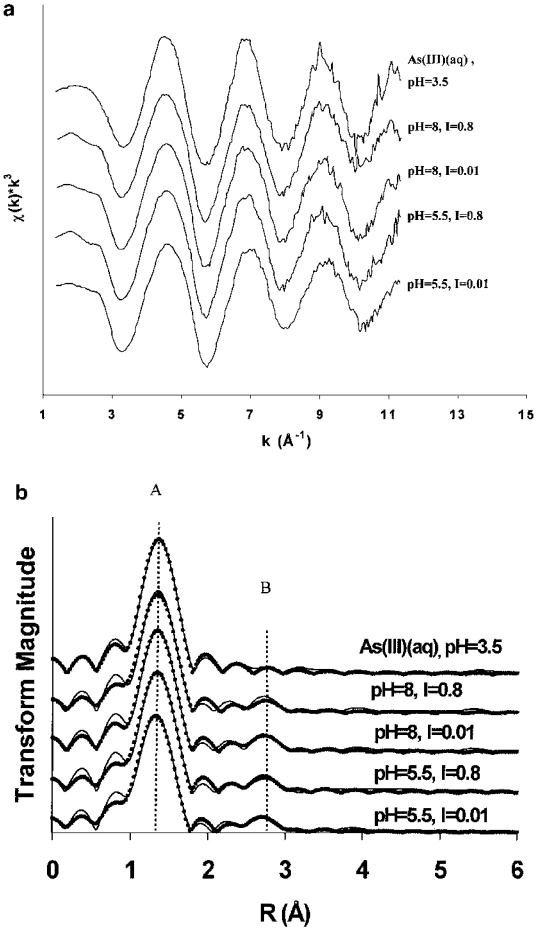

FIG. 6. (a) k^3-weighted normalized χ functions for As(III)(aq) and As(III)/γ-Al_2O_3 adsorption samples. (b) Fourier transforms (RSF) of the χ functions of As(III)/γ-Al_2O_3 adsorption samples. The solid lines are the experimental data and the dotted lines represent the theoretical multishell fit to the data.

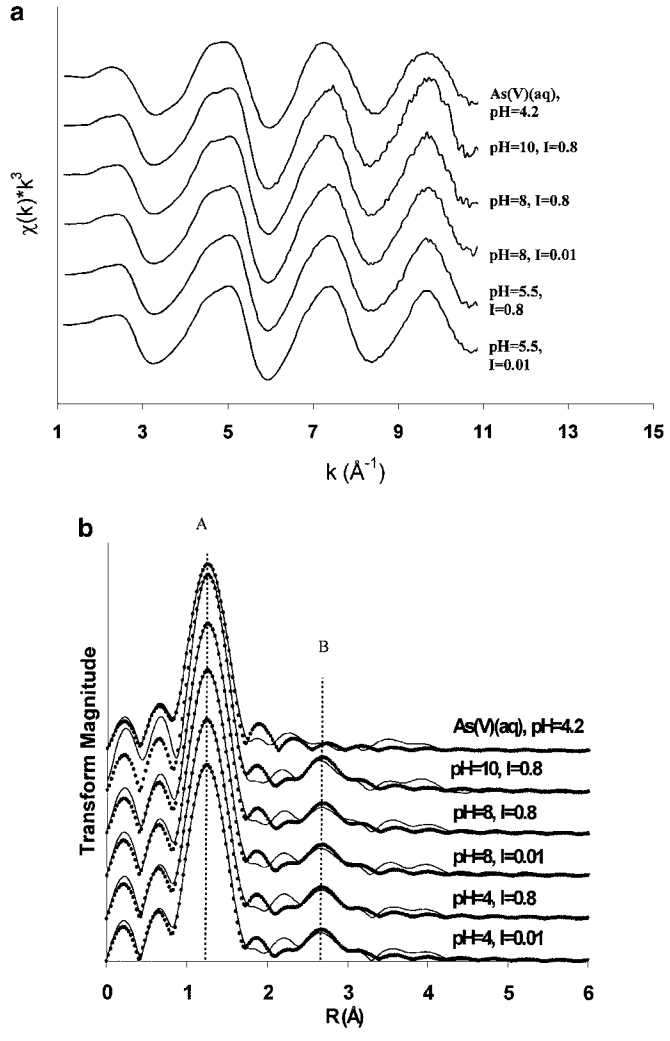

FIG. 7. (a) k^3-weighted normalized χ functions for As(V)(aq) and As(V)/γ-Al_2O_3 adsorption samples. (b) Fourier transforms (RSF) of the χ-functions of As(V)/γ-Al_2O_3 adsorption samples. The solid lines are the experimental data and the dotted lines represent the theoretical multishell fit to the data.

and the As(III and V) solution samples. The spectra show strong sinusoidal oscillations resulting from O-shell backscattering.

Figures 6b and 7b show the RSFs (uncorrected for phase shift) of the As(III and V) solutions and adsorption samples. The solid lines represent the Fourier transforms of the experimental data and the dashed lines are the best fits obtained from multiple-shell fittings. The vertical dashed lines A and B correspond to the As–O and As–Al shells, respectively.

The structural parameters obtained from the linear least-square fits of the EXAFS data are shown in Table 1. The radial distances of As–Al shells were ≅3.22 Å for As(III) and ≅3.11 Å for As(V). These distances can be used to determine the configuration of As(III) and As(V) inner-sphere complexes forming at the hydrated γ-Al_2O_3 surface. Using a known Al–O distance of the AlO_6 octahedral (1.85 to 1.97 Å), an O–O edge separation distance of 2.52–2.86 Å (34), and the experimental As–O distances, the theoretical As–Al bond distances were estimated for different As adsorption configurations (e.g., monodentate, bidentate mononuclear, and bidentate binuclear), assuming that the surface structure of γ-Al_2O_3 (i.e., aluminum tetrahedral configuration) was fully converted to the aluminum octahedral configuration of the bayerite polymorph after 7 days of hydration.

The presence of an Al shell in all samples indicates that As(III) and As(V) inner-sphere complexation occurs under all conditions studied (Figs. 6b and 7b). For monodentate inner-sphere complexation (Figs. 8c and 8f), the $R_{As(III)–Al}$ range is calculated to be 3.62–3.74 Å and the $R_{As(V)–Al}$ range 3.54–3.66 Å. For bidentate mononuclear bonding (Figs. 8b and 8e), the $R_{As(III)–Al}$ range is 2.21–2.75 Å and the $R_{As(V)–Al}$ range is 2.07–2.64 Å. For bidentate binuclear complexation (Figs. 8a and 8d), the $R_{As(III)–Al}$ range is 3.16–3.51 Å and the $R_{As(V)–Al}$ range is 3.03–3.41 Å. The average As–Al distances of the experimental samples as determined by EXAFS (≅3.21 and ≅3.11 Å for As(III) and As(V), respectively) are therefore consistent with inner-sphere bidentate binuclear complexes for both As(III) and As(V). Our XANES data indicated that a mixture of inner-sphere and outer-sphere As(III) complexes was present at pH 8 and $I = 0.01$ M. We do not, however, observe the resultant lower average N_{Al} we would expect as a result of the presence of outer-sphere complexes for this sample compared to those of the other As(III) samples (Table 1). This indicates that the EXAFS data for these spectra are not very sensitive to changes with respect to the Al coordination shell, which is probably due to the weak backscattering of the light Al atom, leading to relatively high uncertainties in N_{Al}. This illustrates the usefulness of combining macroscopic techniques with XANES and EXAFS data in investigating metal/metalloid speciation at mineral/water

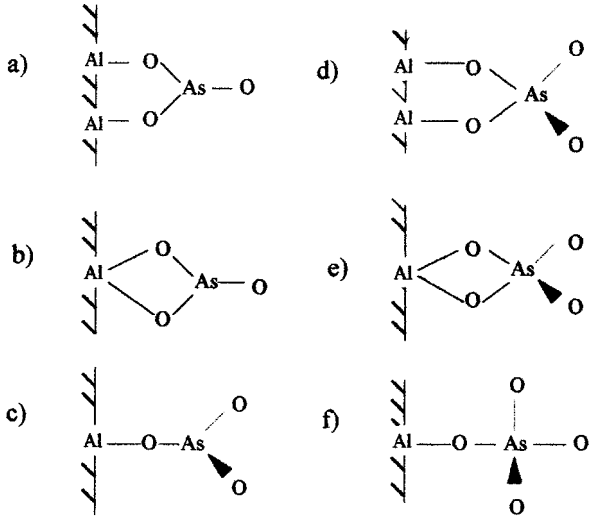

FIG. 8. Molecular configurations of As(III) and As(V) inner-sphere surface complexes. (a) As(III) bidentate binuclear, (b) As(III) bidentate monounclear, (c) As(III) monodentate mononuclear, (d) As(V) bidentate binuclear, (e) As(V) bidentate mononuclear, and (f) As(V) monodentate mononuclear.

TABLE 1
Structural Parameters from XAFS Analysis for As(III and V)/γ-Al_2O_3, Adsorption, and As(III and V) Solution Samples

	As(III)–O			As(III)–Al			
Sample	CN[a,d]	R (Å)[b,e]	σ^2 (Å^2)[c]	CN[f]	R (Å)[g]	σ^2 (Å^2)	E_0 (eV)[d]
As(III)aq, pH = 3.5	3.1	1.78	0.0046				5.58
pH 8, $I = 0.8$	3.0	1.78	0.0054	0.9	3.22	0.01[h]	5.75
pH 8, $I = 0.01$	3.0	1.77	0.0060	1.3	3.22	0.01[h]	5.61
pH 5.5, $I = 0.8$	3.2	1.77	0.0067	1.2	3.19	0.01[h]	5.77
pH 5.5, $I = 0.01$	3.2	1.75	0.0077	1.1	3.19	0.01[h]	5.48
	As(V)–O			As(V)–Al			
Sample	CN[a,d]	R (Å)[b,e]	σ^2 (Å^2)[c]	CN[f]	R (Å)[g]	σ^2 (Å^2)	E_0 (eV)[d]
As(V)aq, pH 4	4.0	1.68	0.0040				3.36
pH 10, $I = 0.8$	4.0	1.69	0.0020	2.2	3.11	0.006[h]	3.58
pH 8, $I = 0.8$	4.1	1.69	0.0025	2.1	3.12	0.006[h]	3.76
pH 8, $I = 0.01$	4.0	1.69	0.0026	2.1	3.11	0.006[h]	3.58
pH 4, $I = 0.8$	4.0	1.68	0.0030	2.1	3.11	0.006[h]	3.63
pH 4, $I = 0.01$	3.9	1.68	0.0029	2.1	3.11	0.006[h]	3.50

[a] Coordination number.
[b] Interatomic distance.
[c] Debye–Waller factor.
[d] Fit quality confidence limit for parameters, ±20%.
[e] Fit quality confidence limit for parameters, ±0.02 Å.
[f] Fit quality confidence limit for parameters, ±30%.
[g] Fit quality confidence limit for parameters, ±0.03 Å.
[h] Fixed parameter.

interfaces. The XANES spectra suggest predominantly inner-sphere As(III) complexation at pH 5.5 and $I = 0.8$ M. The $N_{\text{As–Al}}$ value found for this sample, however, is significantly lower than the $N_{\text{As–Al}}$ values found for the As(V)/alumina spectra, despite the similar molecular configurations of the inner-sphere complexes of As(V) and As(III). This suggests a higher degree of disorder in the population of inner-sphere As(III) complexes, which may lead to destructive interference and therefore an apparent decrease in second-neighbor Al scattering.

SUMMARY

In this study we demonstrated the effectiveness of combining macroscopic (*I*-dependent pH adsorption envelopes and EM measurements) and spectroscopic studies (XANES and EXAFS) in investigating surface complexation mechanisms of As(III) and As(V) at the aluminum oxide/water interface.

Our results suggest that (1) a mixture of inner- and outer-sphere As(III) complexes exist at a pH of >5.5, where outer-sphere As(III) complexes become more important with decreasing I, (2) As(III) predominantly forms inner-sphere bidentate binuclear complexes at a pH of ≤5.5, and (3) As(V) predominantly forms inner-sphere bidentate binuclear complexes regardless of pH and *I*. The co-existence of As(III) inner- and outer-sphere adsorption complexes may be important in predicting the fate and transport of As(III) in Al–oxide-rich environments.

ACKNOWLEDGEMENTS

The authors are grateful to the DuPont Co. for financial support of this research. Y.A. appreciates the receipt of a College of Agricultural and Natural Resources Graduate Research Assistantship and expresses gratitude to Dr. Steve Dentel and Christopher A. Walker for assistance with the EM measurements and to Dr. Rick Maynard of DuPont Co. for assistance with surface area analysis.

REFERENCES

1. Anderson, M. A., Ferguson, J. F., and Gavis, J., *J. Colloid Interface Sci.* **54,** 391 (1976).
2. Raven, K. P., Jain, A., and Loeppert, R. H., *Environ. Sci. Technol.* **32,** 344 (1998).
3. Xu, H., Allard, B., and Grimvall, A, *Water Air Soil Pollut.* **40,** 293 (1988).
4. Walsh, L. M., and Keeny, D. R., *in* "Arsenical pesticides" (E. A. Woolson, Ed.), p. 35. Am. Chem. Soc., Washington DC, 1975.
5. Onishi, H., "Arsenic." Springer-Verlag, New York, 1969.
6. People, S. A. (1975) Review of arsenical pesticides, 1–12.
7. Westcot, D. W., Chilicott, J. E., and Smith, G., "Pond water, sediments and crystal chemistry." ASCE, New York, 1993.
8. Whitacre, R. W., and Pearse, C. S., *Colorado School Mines Miner. Ind. Bull.* **17**(3) (1974).
9. Wagman, D. D., Evans, H. H., Parker, V. B., Schumm, R. H., Harlow, I., Bailey, S. M., Churney, K. L., and Butall, R. L., *J. Phys. Chem. Ref. Data II Suppl.* **2,** 392 (1982).
10. Sposito, G., "The chemistry of soils." Oxford Univ. Press, New York, 1989.
11. Manning, B. A., Fendorf, S. E., and Goldberg, S., *Environ. Sci. Technol.* **32,** 2383 (1998).
12. Manning, B. A., and Goldberg, S., *Environ. Sci. Technol.* **31**(7), 2005 (1997).
13. Hsia, T. H., Lo, S. F., and Lin, C. F., *Chemosphere* **25**(12), 1825 (1992).

14. Fendorf, S. E., Eick, M. J., Grossl, P., and Sparks, D. L., *Environ. Sci. Technol.* **31**(2), 315 (1997).
15. Waychunas, G. A., Rea, B. A., Fuller, C. C., and Davis, J. A., *Geochem. Cosmochim. Acta* **57,** 2251 (1993).
16. Suarez, D. L., Goldberg, S., and Su, C., *in* "Mineral–water interfacial reactions kinetics and mechanisms" (D. L. Sparks and T. J. Grundl, Eds.), p. 136. Am. Chem. Soc. ACS Symposium Series 715, Washington DC, 1998.
17. Sun, X., and Doner, H. E., *Soil Sci.* **161**(12), 865 (1996).
18. Goldberg, S., Davis, J. A., and Hem, J. D., *in* "The environmental chemistry of aluminum" (G. Sposito), p. 271. CRC Press, Boca Raton, FL, 1995.
19. Jacobs, L. W., Syers, J. K., and Keeney, D. R., *Soil Sci. Soc. Am. Proc.* **34,** 750 (1970).
20. Livesey, N. T., and Huang, P. M., *Soil Sci.* **131**(2), 88 (1981).
21. Dyer, C., Hendra, P. J., Forsling, W., and Ranheimer, M., *Spectrochim. Acta Part A*—**49**(5–6), 691 (1993).
22. Wijnja, H., and Schulthess, C. P., *Spectrochim. Acta Part A* **55,** 861 (1999).
23. Cummings, D. E. F., Caccavo, J., Fendorf, S., and Rosenzweig, R. F., *Environ. Sci. Technol.* **33**(5), 723 (1999).
24. Hiemenz, P. C., and Rajagopalan, R., "Electrophoresis and other electrokinetics phenomena." Dekker, New York, 1997.
25. Schecher, W. D., and McAvoy, D. C., MINEQL+ Environmental Research Software. (1998).
26. Ressler, T., *J. Synchrotron Rad.* **5,** 118 (1997).
27. Zabinsky, S. I., Rehr, J. J., Ankudinov, A., Albers, R. C., and Eller, M. J., *Phys. Rev. B* **52**(4), 2995 (1995).
28. Kitahama, K., Kiriyama, R., and Baba, Y., *Acta Crystallogr B* **31,** 322 (1975).
29. Hayes, K. F., Papelis, C., and Leckie, J. O., *J. Colloid Interface Sci.* **125**(2), 717 (1988).
30. Papelis, C., and Hayes, K. F., *Colloids Surf. A* **107,** 89 (1996).
31. Peak, D., Ford, R. G., and Sparks, D. L., *J. Colloid Interface Sci.* **218,** 289 (1999).
32. Strawn, D. G., and Sparks, D. L., *J. Colloid Interface Sci.* **216,** 257 (1999).
33. Hunter, R. J., *in* "Colloid science, A series of monographs." p. 219. Academic Press, San Diego, 1981.
34. Ishizawa, N., Miyata, T., Minato, I., Marumo, F., and Iwai, S., *Acta Crystallogr. C* **36,** 228 (1980).